Maximum Likelihood Estimation of Motor Unit Firing Pattern Statistics

Javier Navallas, Armando Malanda, and Javier Rodriguez-Falces

***Abstract*—Estimation of motor unit firing pattern statistics is a valuable method in physiological studies and a key procedure in electromyographic (EMG) decomposition algorithms. However, if any firings within the pattern are undetected or missed during the decomposition process, the estimation procedure can be disrupted. In order to provide an optimal solution, we present a maximum likelihood estimator of EMG firing pattern statistics, taking into account that some firings may be undetected. A model of the inter-discharge interval (IDI) probability density function with missing firings has been employed to derive the maximum likelihood estimator of the mean and standard deviation of the IDIs. Actual calculation of the maximum likelihood solution has been obtained by means of numerical optimization. The proposed estimator has been evaluated and compared to other previously developed algorithms by means of simulation experiments and has been tested on real signals. The new estimator was found to be robust and reliable in diverse conditions: IDI distributions with a high coefficient of variance or considerable skewness. Moreover, the proposed estimator outperforms previous algorithms both in simulated and real conditions.**

***Index Terms*—Electromyography, inter-discharge interval (IDI), motor unit firing pattern, motor unit potential train.**

I. Introduction

MOTOR UNITs (MUs) are the functional units in the neuromuscular system, each MU comprising a motoneuron and the set of muscle fibers innervated by it. The set of firing instants of a motoneuron is the MU firing pattern, which can be extracted from electromyographic (EMG) recordings by identifying the motor unit potentials (MUPs) and determining the firing instants for each given motor unit. The time between consecutive discharges in a firing pattern is known as inter-discharge interval (IDI). Characterization and estimation of IDI distributions and their main statistics are used as descriptors of motoneuron activity [1]–[4].

Classical sample estimators for IDI mean and standard deviation (SD) adequately characterize IDI distributions when all the discharges in the MU firing pattern are identified, and outliers corresponding to unlikely IDIs are discarded [5], [6]. Under these ideal conditions, physiologically-derived thresholds are used to define the range of acceptable IDIs, assuming that long IDIs are likely to be produced by cessation of motor-unit discharge, whereas very short IDIs are likely to be produced by detection errors or double discharges [5].

However, in medium-to-high force recordings, it is not always possible to completely identify all the discharges in a MU firing pattern due to the superimposition of MUPs, and some of the firings may go undetected [7], [8]. In these situations, EMG decomposition algorithms, which to some extent are able to resolve superimpositions, provide a way to enhance detection of the MU firing pattern [9]–[12] and extract more firing patterns from the same EMG recording. EMG decomposition algorithms rely not only on MUP shape to classify discharges but also on the MU firing pattern information. Consequently, detection of otherwise missed firings by means of IDI statistics estimation provides a fundamental approach to validate and refine the process of EMG decomposition [13]–[15]. In fact, refinement of MUP identification and classification has been a main goal in recent studies, in which new techniques reliant on IDI statistics have been developed [16]–[19].

Several algorithms have been derived to estimate IDI statistics from trains with missing firings [15], [20], [21]. Like the algorithms based on classical sample estimators, an upper and lower threshold is established to define a region of accepted IDIs. In this way an attempt is made to exclude IDIs comprising missing firings and to discard IDIs likely to be produced by misclassifications. However, in these algorithms, thresholds are not predefined but calculated algorithmically from the IDI sample information. One of the main drawbacks of using these approaches is that the number of IDIs used for the final estimation can be considerably reduced if some of the MU firings are not detected. Additionally, there is little certainty that all valid IDIs are included and that all IDIs comprising missing firings are excluded within the set of accepted IDIs.

The goal of this study is to provide an algorithm based on maximum likelihood estimation (MLE) techniques to obtain more robust IDI statistics from a MU firing pattern with undetected firings. In order to do this, the IDI probability density function (PDF) model developed in [20] is used as the likelihood function for the IDIs. This PDF model is based on 1) the MU firing pattern IDI statistics (i.e., the IDI mean and SD) and 2) the probability of detecting individual firings during the detection process. Optimization techniques are employed to obtain the best set of values for the IDI mean, SD and firing detection probability, in terms of likelihood maximization. The algorithm developed uses all the available IDIs in the sample to obtain the final estimation. The new estimator is compared to two previous algorithms: a median-based trimming (MnT) algorithm [15] which is used as a fast estimator of the IDI statistics, and to the error-filtered estimation (EFE) algorithm, which

Manuscript received May 15, 2013; revised October 23, 2013, January 28, 2014; accepted March 05, 2014. Date of publication March 12, 2014; date of current version April 28, 2014.

The authors are with the Department of Electrical and Electronic Engineering, Public University of Navarra, 31006 Navarra, Spain (e-mail: javier.navallas@unavarra.es).

Digital Object Identifier 10.1109/TNSRE.2014.2311502

TABLE I
RANGES AND VALUES FOR THE IDI PDF PARAMETERS

Param.	Physiological range	Optimiz. range	Initial guess
μ	30 - 160 ms (see [2], [3])	$[0, \infty)$	mode(τ_i)
σ	5 - 25 ms (see [2], [3])	$[0, \infty)$	0.2 mode(τ_i)
p	-	[0, 1]	0.5

has been shown to be more robust and reliable than other previously derived estimators [21]. Performance is tested with both simulated data and real signals. The conditions of applicability and essential advantages of the proposed model are discussed, and the current paper closes with our conclusions.

II. METHODS

A. Physiological Basis

Mathematically, firing times within a MU firing pattern can be regarded as the result of a stochastic process, more precisely a stochastic point process, as firing times are completely defined by their time of occurrence [2]. On the basis of physiological evidence, the MU firing pattern stochastic process is essentially nonstationary, because the mean firing rate tends to increase with increased degree of voluntary contraction [22], and the firing rate variability tends to decrease above the recruitment threshold [2], [3], remaining constant for higher force levels [5]. Even in constant force isometric contractions, if these are sustained, the firing rate tends to decrease while the force twitch duration increases for individual motor units, as a result of adaptation to fatigue [23]. However, the process can be considered stationary in short duration contractions [21], that is, when contraction is sustained for less than 10 s [1]. If stationary conditions are assumed, IDIs can be modeled as random variables identically distributed according to a certain PDF.

There is conflicting evidence about the dependency between IDIs. Some experimenters have found no dependency between adjacent IDIs [2], [24] or no significant dependency [25], while other experimenters have found negative dependency between adjacent IDIs [26], and negative dependency only for high firing rates over 13 pulses/s [3]. A negative correlation would indicate that large IDIs tend to be followed by short ones and vice versa. If stationarity and independence are assumed, IDIs can be considered independent and identically distributed according to a certain PDF, and the MU firing pattern can be modeled as a renewal process.

Studies of statistical characterization of IDI distributions have focused on the mean and standard deviation (SD) values (Table I), and also on the shape in terms of the degree of symmetry, as measured by the skewness. Regarding the mean and SD values, reports indicate a normal range from 30 to 160 ms for the mean, and from 5 to 25 ms for the SD [2], [3]. In addition, the SD tends to decrease for lower mean IDI values [3], [25]. Reported coefficient of variation (CV) values range from 0.1 to 0.33 [2]. Reports on PDF shape differ: some researchers found highly symmetrical distributions [2], [27], while others found slight or moderate positive skewness [3], [25]. The latter researchers reported that skewness decreased for lower mean IDI values, meaning that symmetrical IDI distributions were found at high firing rates [3]. However, asymmetry can arise from the nonstationary nature of conditions that result from the experimental setup [1], [4]. In an attempt to accommodate all the above disparate evidence, the IDI PDF has previously been modeled as a normal distribution [4], [20], [21], but also as a gamma distribution, which allows control of skewness [4].

B. Derivation of the MLE

In our model, it is assumed that during constant force isometric contractions of short duration, firings from a MU firing pattern, t_i, can be modeled as a renewal point process. The corresponding IDIs, which are defined as the time intervals between firings, $\tau_i = t_{i+1} - t_i$, can be assumed to be independently and identically distributed following a normal distribution with mean, μ, and SD, σ. Hence, the MU firing pattern is a discrete set of firings at times $\{t_i\}_{i=1}^{N+1}$, and the IDIs, $\{\tau_i\}_{i=1}^{N}$, follow a normal distribution, $N(\tau_i|\mu, \sigma)$.

The detection process is defined as the procedure to extract the MU firing pattern from the EMG signal. Each of the firing instants will be detected with some detection probability, p. If we assume that the detection of each firing is independent from each other, the probability of finding an IDI where $k-1$ firings are missing is $p(1-p)^{k-1}$, and the IDI being measured will be the summation of k individual IDIs distributed as $N(\mu, \sigma)$, leading to a normal distribution of $N(\mu k, \sigma\sqrt{k})$. Hence, the IDI PDF after a firing detection process with a detection probability p is [20]

$$f(\tau_i) = \sum_{k=1}^{\infty} p(1-p)^{k-1} N(\tau_i|\mu k, \sigma\sqrt{k}). \quad (1)$$

In an experiment of limited duration, only a finite number of firings are identified. Hence the sample of IDIs will contain a limited number of observations. Given a set of N IDI observations we can obtain its joint PDF as

$$f(\tau_1, \ldots, \tau_n) = \prod_{i=1}^{N} \sum_{k=1}^{\infty} p(1-p)^{k-1} N(\tau_i|\mu k, \sigma\sqrt{k}). \quad (2)$$

For a given set of parameters, (μ, σ, p), this is the likelihood function of the parameters given the IDI observations, $L(\mu, \sigma, p|\tau_1, \ldots, \tau_n)$. The maximum likelihood estimator of the distribution parameters, $(\hat{\mu}, \hat{\sigma}, \hat{p})$, can be obtained by maximizing the natural logarithm of (2). The MLE can be determined by applying optimization techniques within a bounded parameter space, given that both μ and σ must be nonnegative, and p must take a value between 0 and 1.

The main problem in applying optimization is that the missing firings density function has infinite terms in its summation. However, the relative importance of each term decreases for increasing order, k, given the term $p(1-p)^{k-1}$, where $p < 1$ (if $p = 1$ then all the discharges are detected and only the first term is required). Hence, the summation may be truncated with a negligible effect on the final result

$$LL(\mu, \sigma, p|\tau_1, \ldots, \tau_n) \approx \sum_{i=1}^{N} \ln \sum_{k=1}^{K} p(1-p)^{k-1} N(\tau_i|\mu k, \sigma\sqrt{k}) \quad (3)$$

where K is the truncation order of the approximation. A maximum order $K = 20$ was chosen on the basis of evaluation tests that are presented in Section III-A.

Special care is required when selecting the starting solution in any optimization process. Following [21], the mode of the IDI histogram can be considered a good first guess for the mean value, while 0.2 times this mean value is a good first guess for the SD, given that physiological values of the CV usually range from 0.1 to 0.3. For the detection probability, a starting value of 0.5 was selected after we had carried out the evaluation tests that are presented in Section III-B.

In the current implementation, the Nelder–Mead simplex optimization method is used with a variable transformation to implement bound constraints. Optimization variables which are constrained by both a lower and an upper bound (p) use a sine transformation, while those constrained by only a lower bound (μ and σ) use a quadratic transformation [29].

C. Evaluation With Simulated MU Firing Patterns

To evaluate the estimator, six groups of simulation experiments were conducted. In each trial of the simulations, for a given set (μ, σ, p) a MU firing pattern is generated with IDIs drawn, unless otherwise specified, from a normal distribution $N(\mu, \sigma)$. The number of IDIs must be high enough to cover a recording time of 5 s. In order to model the real situation where some firings may be missed in the detection process, individual firings are independently discarded with probability $1 - p$. The IDIs between the surviving firings are recalculated, giving the final IDI set. Estimation algorithms are applied to the IDI set, obtaining the mean and SD estimates of the MU firing pattern IDI. The three estimation algorithms employed are two previously proposed algorithms: the MnT [15] and the EFE [21]; and the MLE approach introduced in this study.

Evaluation of the different algorithms is performed by calculating the normalized estimation error for every trial

$$\epsilon_\mu = (\hat{\mu} - \mu)/\mu,\ \epsilon_\sigma = (\hat{\sigma} - \sigma)/\sigma \tag{4}$$

where ϵ_μ and ϵ_σ stand for the IDI mean and SD normalized estimation errors, μ and σ stand for the real IDI mean and SD, $\hat{\mu}$ and $\hat{\sigma}$ stand for the estimated IDI mean and SD.

The mean of the normalized estimation errors is calculated, being a measure of the estimation bias. The 25, 50, and 75 percentiles of the normalized estimation errors are also calculated, being a measure of the variability range and distribution shape of the estimation errors. Additionally, the 1.5 interquartile range (IQR) and the set of outliers are calculated for further characterization of the dispersion of estimation errors.

The six groups of simulation experiments are detailed next.

1) Influence of the PDF Truncation Order: In order to determine the effect of truncation of the missing firings distribution, the maximum order, K, is varied between 5 and 40 in steps of 5, while the detection probability is varied from 1 down to 0.2 in steps of 0.05. For each combination, 10 000 trials are simulated with the mean and SD of the IDIs randomly selected from the ranges given in Table I.

2) Influence of the Initial Conditions: In order to determine the influence of the initial value of the detection probability, p, this value is varied between 0 and 1 in steps of 0.1, while the detection probability is varied from 1 down to 0.2 in steps of 0.05. For each combination, 10 000 trials are simulated with the mean and SD of the IDIs randomly selected from the ranges given in Table I.

3) Influence of the CV: In order to determine the influence of the CV, three different values are employed: 0.1, 0.2, and 0.3, while the detection probability is varied between 0.2 and 1 in steps of 0.2. For each combination, 10 000 trials are simulated with the mean of the IDIs randomly selected from the range given in Table I, and the corresponding SD calculated according to the selected CV.

4) Influence of IDI PDF Skewness: When testing the algorithm with skewed IDI distributions, a gamma PDF is used to generate the synthetic IDI data instead of a normal distribution. The generalized version presented in [4] allowing for independent control of the mean, SD, and skewness is employed

$$f(\tau_i) = \frac{1}{\beta\Gamma(\theta)}\left(\frac{x-\alpha}{\beta}\right)^{\theta-1}\exp\left(-\frac{x-\alpha}{\beta}\right) \tag{5}$$

where α is the location parameter, β is the scale parameter, and θ is the shape parameter. In order to fit these parameters as a function of the desired mean, μ, SD, σ, and skewness, γ, the following relationships are employed:

$$\alpha = \mu - 2\sigma/\gamma,\ \beta = \sigma\gamma/2,\ \theta = 4/\gamma^2. \tag{6}$$

In order to determine the influence of the skewness of the IDI distribution, the gamma PDF is used with two different skewness values (0.5 and 1.0), while the missed detection probability is varied between 0.2 and 1 in steps of 0.2. For each combination, 10 000 trials are simulated with the mean and SD of the IDIs randomly selected from the range given in Table I, and the corresponding parameters of the gamma PDF calculated as in (6).

5) Influence of the MU Firing Pattern Length: In order to determine the influence of the number of IDIs of the sample, N, the length of the MU firing pattern is varied between 5 and 120 s in steps of 5 s. For each value, 1000 trials are simulated with the mean of IDIs being fixed at 100 ms, the detection probability randomly selected between 0.3 and 1.0, and the SD of the IDIs randomly selected from the range given in Table I. Given that the mean IDI is kept fixed throughout this simulation, by varying the length of the MU firing pattern, the number of IDIs in the complete pattern (prior to attempted detection of firings) is proportionally varied. In addition to the normalized estimation errors, a rough measurement of the computational cost per trial is obtained by averaging the computation time within each set of 1000 trials.

6) Reliability of the Estimation Methods: In order to determine the range of the MU firing pattern parameters, p and CV, within which each algorithm may be considered reliable, the detection probability is varied between 0.3 and 1 in steps of 0.05, while the CV is varied between 0.1 and 0.4 in steps of 0.025. For each combination, 1000 trials are simulated with the mean of the IDIs randomly selected from the range given in Table I, and the algorithm is considered reliable if the error is lower than 15% in at least 90% of the trials for the IDI mean and at least

70% of the trials for the IDI SD. The small steps used in the simulation allow depiction of reliability maps.

D. Evaluation With Real MU Firing Patterns

For evaluation with real MU firing patterns, real EMG signals recorded with concentric needle electrodes are employed. Signals of 10 s duration are recorded during low force isometric contractions, from the rectus femoris and vastus medialis muscles of healthy subjects. Complete MU firing patterns, used as ground truth, are obtained by manual decomposition in the EMGLab environment [28]. Incomplete MU firing patterns used to test the estimation algorithms are obtained by means of an automatic decomposition algorithm [28], that may miss some of the firings or include extra firings not belonging to the actual MU due to decomposition errors. The number of identified MU firing patterns per signal simultaneously detected by both processing methods ranges from 2 to 6. Highly nonstationary MU firing patterns are discarded from the evaluation procedure. For each MU firing pattern, the IDIs are calculated, resulting in a total of 126 IDI sets. The number of detected IDIs per firing pattern ranges from 51 to 136 in the complete firing patterns, and from 11 to 119 in the incomplete firing patterns.

The IDI mean and SD are estimated by applying the three algorithms to the incomplete firing patterns. The IDI sample mean and sample SD of the complete firing patterns are obtained as the ground truth values for calculating the normalized estimation errors of the three algorithms. In order to study the performance for different detection probabilities, for each incomplete pattern, p is calculated as the ratio of the number of firings in the incomplete pattern to that in the corresponding complete pattern.

Normality of the IDI sample of the complete patterns is tested with a Lilliefors test (significance level: $\alpha = 0.01$) and 88 of the 126 MU firing patterns remain compatible with a normal IDI distribution. In order to test the goodness-of-fit of a normal distribution with the parameters estimated from the incomplete MU firing patterns, Kolmogorov–Smirnov test (significance level: $\alpha = 0.05$) is performed after each estimation; the null hypothesis being that the IDI sample of the complete pattern is drawn from a normal distribution with population parameters $\hat{\mu}$ and $\hat{\sigma}$ obtained from estimation. Rejection of the null hypothesis in the Kolmogorov–Smirnov test indicates that the IDI mean and SD estimated by the algorithm fail to model the complete IDI sample as drawn from a normal distribution, while the Lilliefors test has not discarded the possibility of the complete IDI sample being drawn from a normal distribution.

III. Results

A. Influence of the PDF Truncation Order

In order to characterize the behavior of the IDI mean and SD estimators, the estimation bias is depicted as a function of the missed-detection probability, $1 - p$, for different values of the truncation limit (Fig. 1).

The results of our tests on the influence of the PDF truncation order show that as the misdetection probability increases a higher truncation limit is needed (Fig. 1). These results also show that incrementing K above 20 does not provide an appreciable improvement of the estimation performance, either in terms of the bias or in terms of the variability. On this basis we chose a fixed limit of $K = 20$ for our evaluative tests; this being the best trade-off between computational cost and estimation performance.

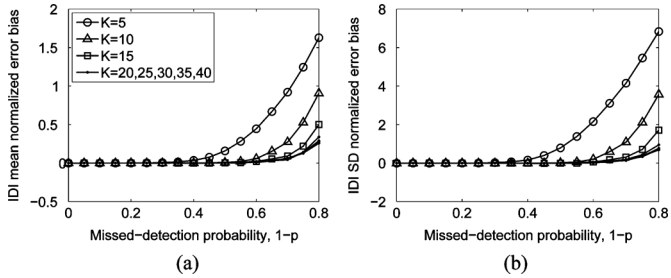

Fig. 1. Performance of the MLE for different values of the truncation limit, K, as a function of the detection probability: (a) mean error of the IDI mean estimate; (b) mean error of the SD estimate. Note that mean errors were similar (independent of K) when K was 20 or greater.

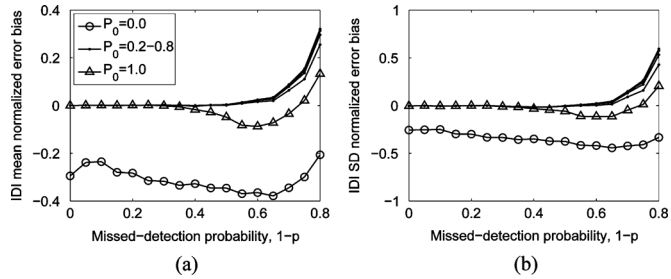

Fig. 2. Performance of the MLE for different values of the initial detection probability, p, as a function of the detection probability: (a) mean error of the IDI mean estimate; (b) mean error of the SD estimate. Note that mean errors were similar (independent of p) when the initial value of p was in the range 0.2 to 0.8.

B. Influence of the Initial Conditions

Results of tests directed at evaluating the dependency of the MLE on the initial detection probability, p, show that estimator performance was similar across the range of possible initial values except at the extremes (i.e., 0 and 1) of the range (Fig. 2). Hence, a value of 0.5 was selected as the starting point for the optimization procedure.

C. Influence of the IDI PDF CV

Figs. 3 and 4 show the influence of the IDI PDF CV on the estimation error of the IDI mean and SD, respectively. In the figures, each row corresponds to a different CV value, and each column to a different value of the detection probability. Within each subplot, the distribution of the normalized errors of the three algorithms are compared by means of box plots. Observing the overall results for the mean IDI (Fig. 3) and the IDI SD estimation (Fig. 4), an increase in the error dispersion as the detection probability decreases can be observed for the three algorithms; note the change of scale in the error plots. In the case of the mean IDI, the error dispersion also tends to increase as the CV increases, although this increase becomes less evident as the detection probability decreases.

In terms of estimation of the IDI mean (Fig. 3), the MLE algorithm shows a lower bias than the MnT and EFE algorithms. While the MnT algorithm becomes positively biased even with

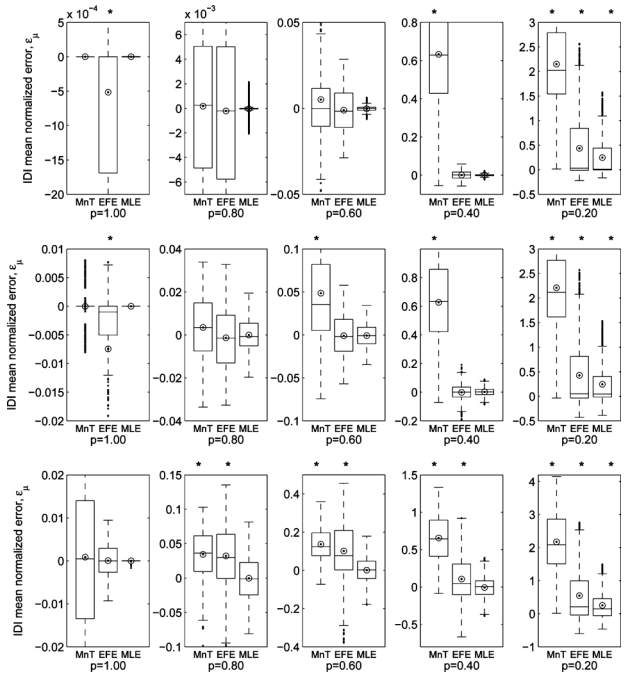

Fig. 3. Normalized error of the IDI mean, ϵ_μ, for the three algorithms (MnT, EFE, and MLE) with different combinations of the firing detection probability, p (decreasing from left to right) and the CV ($\mathrm{CV} = 0.1$ in the upper row; $\mathrm{CV} = 0.2$ in the middle row; and $\mathrm{CV} = 0.3$ in the lower row). In each plot, results from the distribution of the error in the three algorithms are summarized in terms of the mean value (encircled dot), the 25, 50, and 75 percentiles (boxes), the ± 1.5 IQR (whiskers), and the outliers (dots outside the whiskers range). Additionally, the star above some boxplots indicate that the distribution of the error is markedly biased (i.e., the mean error is far from 0 for the scale shown or the IQR does not containing the 0 value).

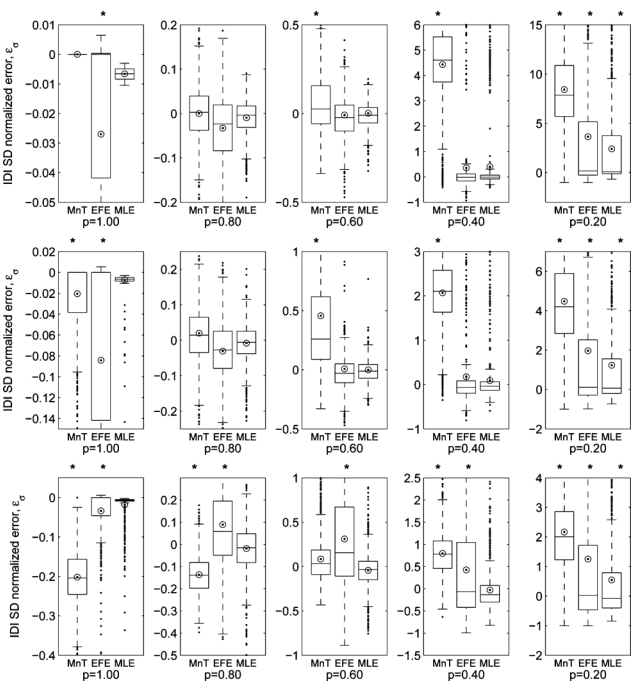

Fig. 4. Normalized error of the IDI SD, ϵ_σ, for the three algorithms (MnT, EFE, and MLE) with different combinations of the firing detection probability, p (decreasing from left to right) and the CV ($\mathrm{CV} = 0.1$ in the upper row; $\mathrm{CV} = 0.2$ in the middle row; and $\mathrm{CV} = 0.3$ in the lower row). Symbols used in the plots are the same as in Fig. 3.

moderate p and CV values, and while the EFE algorithm becomes biased with the highest and lowest p values tested, the MLE algorithm only becomes biased with the lowest p values. MLE estimation, even when biased, still has lower bias than the other two algorithms. Note that the MLE remains unbiased for $p = 0.4$ and $\mathrm{CV} = 0.3$, while the other algorithms are showing bias even for p values greater than 0.4. The variability of error in IDI mean estimation is also smaller with the MLE algorithm for all the combinations of p and CV tested. Especially noticeable is the difference with high p values and low CV values, where the dispersion of the MLE is up to 10-fold smaller than that of the MnT and EFE algorithms.

In terms of the IDI SD estimation (Fig. 4), the MLE algorithm also shows a lower bias and a smaller dispersion than the MnT and EFE algorithms for all the combinations of p and CV being tested. Again, MLE outperforms MnT and EFE algorithms when the p value is at its highest $(p = 1)$ and when CV values are small. All three algorithms present a considerable number of outlying estimations: they tend to underestimate the IDI SD value when p is high, and tend to overestimate it when p is moderate to low.

D. Influence of the IDI PDF Skewness

Figs. 5 and 6 show the influence of skewness in the IDI PDF on the estimation error of the IDI mean and SD, respectively. In the figures, each row corresponds to a different skewness value and each column to different values of the detection probability, p. In each subplot, the distributions of the normalized error of the three algorithms are compared by means of box plots. The results show, for all three algorithms, an increase in the error dispersion as the detection probability decreases. An increase in skewness has a small impact on the performance of the algorithms.

In terms of estimation of the IDI mean (Fig. 5), both the MLE and EFE algorithms show a lower bias than the MnT algorithm. MLE most clearly outperforms the other two algorithms when the p value is highest and there is low skewness. Additionally, the dispersion of the error is lower under MLE than under MnT and EFE for all tested combinations of detection probability and skewness. When skewness is present, the estimation becomes negatively biased for high p values and positively biased for low p values. The contrary occurs for high p values when skewness is absent and the PDF follows a normal distribution: a positive bias is observed (Fig. 3).

With regard to estimation of IDI SD (Fig. 6), the MLE algorithm is less biased and has lower dispersion with all the tested combinations of the detection probability and skewness. With skewness, all three algorithms produce noticeable more outlying SD estimations. However, the error ranges in all the cases are comparable to that of the previous experiment with normally-distributed IDI PDFs.

E. Influence of the MU Firing Pattern Length

Fig. 7 shows the influence of the length of the MU firing pattern on the bias of the estimation error of the IDI mean and SD. As noted before, given that the mean IDI is kept fixed, the length of the MU firing pattern is proportional to the number of IDIs

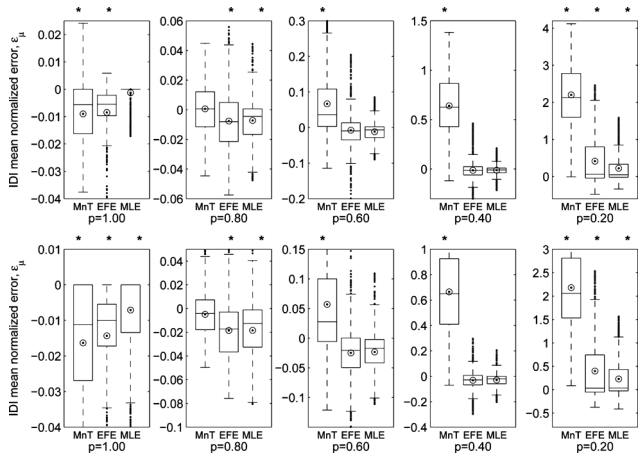

Fig. 5. Normalized error of the IDI mean, ϵ_μ, for the three algorithms (MnT, EFE, and MLE) with different combinations of the firing detection probability, p (decreasing from left to right) and the skewness ($\gamma = 0.5$ in the upper row; and $\gamma = 1.0$ in the lower row). The symbols used in the plots are the same as in Fig. 3.

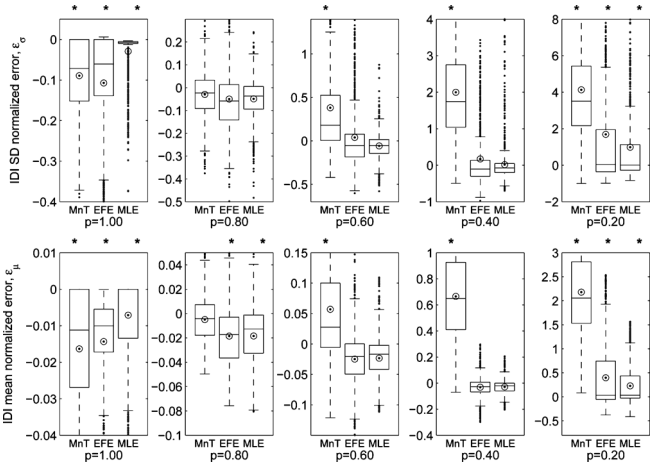

Fig. 6. Normalized error of the IDI SD, ϵ_σ, for the three algorithms (MnT, EFE, and MLE) with different combinations of the firing detection probability, p (decreasing from left to right) and the skewness ($\gamma = 0.5$ in the upper row; and $\gamma = 1.0$ in the lower row). Symbols used in the plots are the same as in Fig. 3.

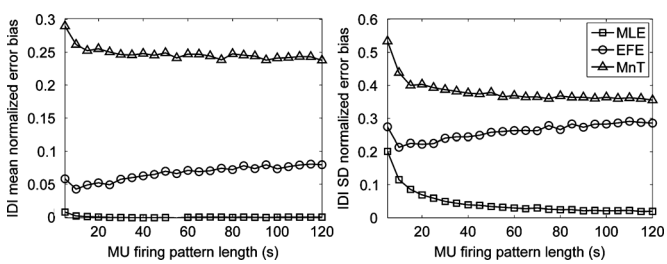

Fig. 7. Bias of the normalized error of the IDI mean and SD, ϵ_μ and ϵ_σ, for the three algorithms (MnT, EFE, and MLE) as a function of the length of the MU firing pattern which is proportional to the number of IDIs, N.

in the complete firing pattern. Results show that the three algorithms lower its error bias as the length increases from 5 to 10 s. However, after this initial enhancement, the behavior of the error bias for the three algorithms is different: MnT error bias slightly decreases with the number of available IDIs; EFE error bias tends to increase with the number of available IDIs;

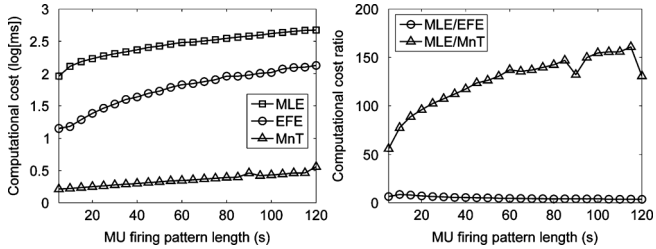

Fig. 8. Computation time per trial for the three algorithms (MnT, EFE, and MLE) and ratios as a function of the length of the MU firing pattern which is proportional to the number of IDIs, N.

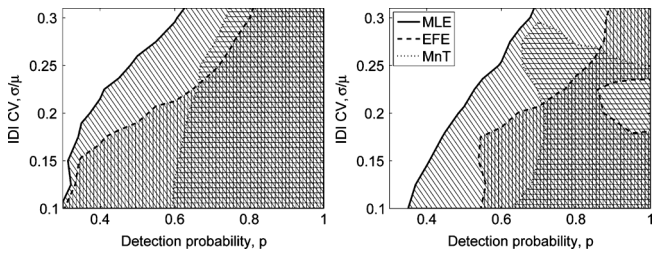

Fig. 9. Reliability maps of the three algorithms (MnT, EFE, and MLE) in the p-CV parameter space. Each algorithm can be considered reliable for a given parameter combination if estimation error is lower than 15% at least 90% of the times for the IDI mean and 70% of the times for the IDI SD. Shaded regions show the p-CV parameter combinations where the MnT (horizontal pattern), EFE (vertical pattern), and MLE (diagonal pattern) are reliable.

and MLE error bias decreases and can be considered unbiased in the estimation of the IDI mean for lengths over 25 s, and it tends towards unbiasedness in the estimation of the IDI SD.

Fig. 8 shows the influence of the length of the MU firing pattern on the computational cost for each algorithm and the cost ratios of the MLE to the EFE and MnT algorithms, respectively. Results show that MnT is the most efficient and MLE the least efficient in the range from 5 to 120 s. For a MU firing pattern length of 10 s, a single estimation takes, on average, 0.18 ms for the MnT, 1.23 ms for the EFE, and 6.02 ms for the MLE. Hence, the MnT algorithm is almost 50 times more efficient than the MLE, and the EFE algorithm is almost five times more efficient than the MLE. The cost of the MLE and EFE algorithms has a linear dependency on N, while the cost of the MnT algorithm has a logarithmic dependency on N; i.e., MnT becomes comparatively more efficient as N increases. As observable in Fig. 8, results show an almost constant cost ratio between the MLE and MnT algorithms, but an increasing cost ratio between the MLE and EFE algorithms as a function of N.

F. Reliability of the Estimation Methods

Fig. 9 shows the regions within the explored p-CV parameter space in which each algorithm shows reliable behavior, as defined in Section II-C6. For the estimation of the IDI mean, MLE is reliable in the widest area, which corresponds to all the explored space except where p is low and CV is high at the same time. The EFE algorithm is also reliable in a wide area, but its reliability decays for CV values over 0.2, where a high detection probability is needed ($p > 0.6$) for the algorithm to be reliable. Finally, the MnT is only reliable for p values over 0.6, being the least sensitive of the three algorithms to CV variations. For estimation of IDI SD, similar results are observed:

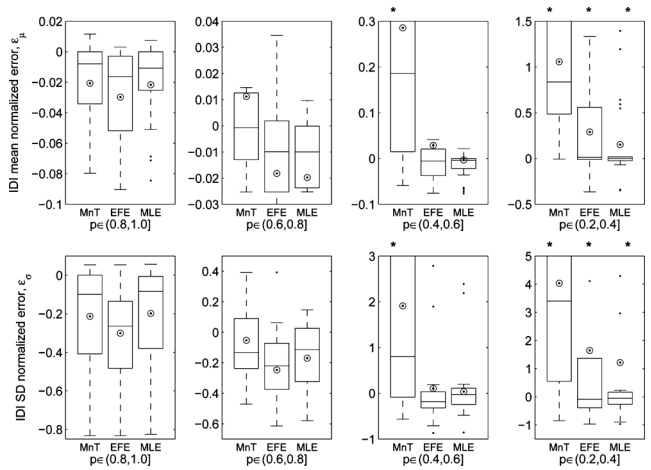

Fig. 10. Normalized error of the IDI mean, ϵ_μ (upper row), and SD, ϵ_σ (lower row), for real MUPTs. Each plot comprises all the real MU potential trains that have p values that fall within the indicated range. Vertical scale has been selected to facilitate comparison between EFE and MLE results (cutting off some of the results for MnT). Symbols are as in Fig. 3.

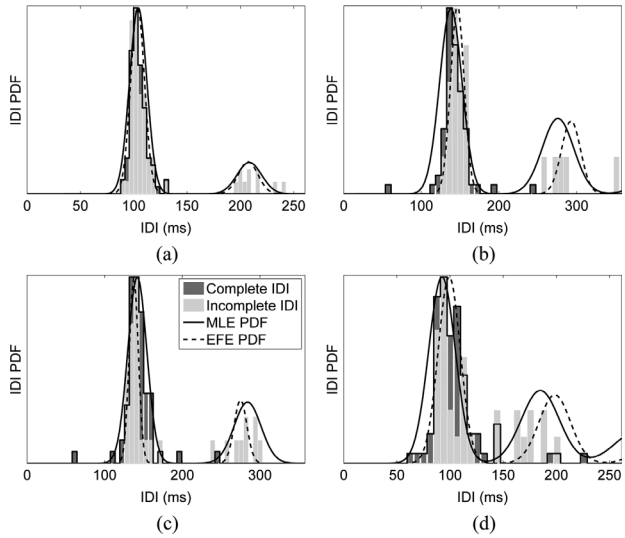

Fig. 11. Four different cases of Kolmogorv-Smirnov tests: (a) MLE and EFE not rejected; (b) MLE and EFE rejected; (c) MLE not rejected and EFE rejected; and (d) MLE rejected and EFE not rejected. In all the cases the figures show the empirical histograms of the complete and incomplete MU firing pattern sets, and the IDI PDF with missing firings from (1) evaluated with the population parameters as estimated from the MLE and EFE algorithms. In the case of the EFE, the detection probability, not provided by the estimation procedure, is alternatively estimated as the identification rate [16]. Note that the PDFs evaluated in the Kolmogorov–Smirnov test are not the ones depicted here, but the normal PDFs corresponding only to the contribution of the first lobes, which are supposed to represent the complete MU firing pattern IDI distribution. IDIs over 2.5 times the mean IDI are not shown for the sake of clarity.

MLE outperforms both EFE and MnT. However, reliability regions are smaller, meaning that the reliability in IDI SD estimation is lower than that in IDI mean estimation.

G. Results With Real MU Firing Patterns

The normalized estimation errors for the three algorithms when applied to real signals are summarized in Fig. 10. Both the MLE and EFE algorithms outperform the MnT algorithm in the estimation of the mean and SD. In comparison to EFE, MLE has smaller dispersion of errors and lower biases than the EFE algorithm for detection probabilities under 0.6, especially in the estimation of IDI mean. These results are comparable to the simulation results obtained when a moderate amount of skewness is introduced in the IDI distributions.

The results from the Kolmogorov-Smirnov test indicate a rejection of the null hypothesis in 19.3% of the signals (17/88) for the MLE algorithm, 38.6% of the signals (34/88) for the EFE algorithm, and 50.0% (44/88) for the MnT algorithm. If stationarity conditions are strengthened and only 32 out of the 88 signals are considered, the null hypothesis is rejected in 12.5% of the signals (4/32) for the MLE algorithm, 31.3% of the signals (10/32) for the EFE algorithm, and 37.5% (12/32) for the MnT algorithm. In both cases the MLE algorithm gives almost half the number of null hypothesis rejections that the EFE and MnT algorithms do. In relaxed stationarity conditions (when 88 signals are kept for analysis), 15 of the 17 rejections of the MLE algorithm are also rejections for the EFE and MnT, and the remaining two cases are rejections both for the MLE and MnT but not for the EFE. As all the MLE and EFE rejections imply a MnT rejection, and for the sake of simplicity, in the following analysis of the results only EFE and MLE are compared.

Fig. 11 shows outcomes of the Kolmogorov–Smirnov tests, which are representative of the four different combinations of null hypothesis rejection and nonrejection for the MLE and EFE algorithms when applied to the same data set. In the two examples where the EFE algorithm estimation is rejected, the cause is an underestimation of the IDI SD, while in the two examples where MLE algorithm estimation is rejected, the cause is a combination of underestimation of the IDI mean and an overestimation of the IDI SD.

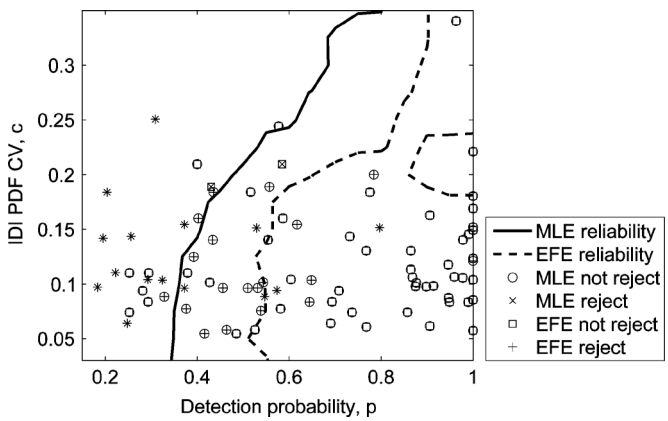

Fig. 12. Outcomes of the Kolmogorov–Smirnov tests for the MLE and EFE algorithms depicted within the p-CV parameter space with the reliability limits obtained for the IDI SD estimation being the same as in Fig. 9. For each real signal, CV is calculated from the complete MU firing pattern statistics, and p is calculated as the ratio of firings in the incomplete pattern to that of the complete pattern. Note that the gain in the MLE over the EFE algorithm ($\oplus$ symbols) is concentrated in a region with moderate detection probability and low CV.

Fig. 12 shows the outcomes of the Kolmogorov-Smirnov tests for the MLE and EFE algorithms depicted within the p-CV space, where CV is calculated from the complete MU firing pattern statistics, and p is calculated as the ratio of IDIs in the incomplete pattern to that of the complete pattern. Both algorithms generally provide accurate outcomes whenever p is over 0.8 or

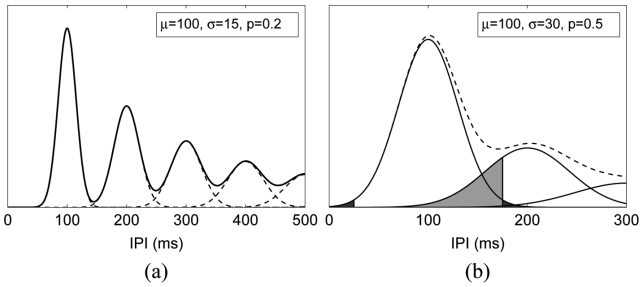

Fig. 13. Missing firings IDI PDF showing the influence of: (a) a low detection probability, that produces a wide spread of the distribution through the different lobes; (b) a high coefficient of variation, that produces a high degree of overlapping of the left tail of the second lobe with the first lobe. If hard limits are used to define a region for statistics calculation, part of the second lobe tail will be inside the region (light gray), while the outermost parts of the first lobe will be missed (dark gray).

CV is under 0.2, while both tend to result in rejection of the null hypothesis with middle to low detection probability values, i.e., when p is under 0.6. The main advantage of the MLE over the EFE algorithm (MLE results in nonrejection while EFE results in rejection) occurs in a region with moderate detection probability (0.4 to 0.6) and moderate to low CV (0.1 to 0.2). This coincides with part of the region where, in terms of IDI SD estimation, MLE is shown to be reliable but the EFE is shown not to be reliable.

IV. Discussion

MLE provides accurate, precise and robust estimates of the mean and SD of the IDI distribution of a MU firing pattern. This is achieved by using all the IDI samples, as opposed to discarding the ones corresponding to missing firing IDIs as previous approaches do. To this end, the MLE uses a PDF model that incorporates the probability of the system detecting individual firings, and this model has been shown to adequately model real IDI samples.

A. Fundamental Aspects of IDI Statistics Estimation

When trying to estimate the IDI statistics from a MU firing pattern with missing firings, two main aspects will affect the observed IDI distribution from which the sample is drawn: the firing detection probability and the coefficient of variation of the real IDI distribution. The detection probability determines the relative weight of the normal distributions centered at $k\mu$ (1), corresponding to IDIs being calculated with $k-1$ missing firings (in the following discussion we will refer to these distributions centered at $k\mu$ as the lobes of the distribution, with the main lobe $(k=1)$ being the one corresponding to IDIs with no missing firings) [Fig. 13(a)]. The lower the detection probability, the higher the relative importance of the side lobes of the distribution. On the other hand, the coefficient of variation determines the width of the distribution lobes in relation to their spacing; while the separation between adjacent lobes is constant and equal to μ, their width increases as $\sigma\sqrt{k}$, hence, in terms of the CV, the width increases as $c\mu\sqrt{k}$. The degree of overlapping, understood as the proportion between lobe width and separation, is $c\sqrt{k}$. Hence, the higher the coefficient of variation, the higher the overlapping. The overlapping that concerns us here is that which interferes with the main distribution lobe (the one centered on μ), and the most important overlapping comes from the left side of the second lobe [Fig. 13(b)].

If an estimation approach relies on the establishment of thresholds in IDI values in order to find the IDIs corresponding to the main lobe [15], [20], [21], two problems arise: first, for high CV values we cannot ensure that the IDIs are not coming from the second lobe; and second, we are discarding a considerable amount of data from the IDI sample, as we are discarding IDIs, hence we are underusing the information provided by the sample. The first effect becomes important for CV values around 0.3, where the 3σ right side of the first lobe completely overlaps with the 3σ left side of the second lobe [Fig. 13(b)]. Hence, half of the second lobe IDIs lie within the first lobe and there is no way to determine which IDIs correspond to which lobe. With a CV of 0.33 and a moderate detection probability of 0.5, 12.5% $(p(1-p)/2)$ of the IDIs actually correspond to the second lobe but lie within the 3σ limits of the first lobe. The second effect becomes worse as the detection probability decreases, because the expected number of IDIs within a sample of size N that correspond to the main lobe is pN, and the IDIs tend to spread through the different lobes [Fig. 13(a)]. For a record of 5 s duration, with a mean IDI of 100 ms, and a detection probability of 0.2, only about 10 IDIs are measured, and only about 2 of these correspond to IDIs within the first lobe; in the best case scenario, if we are able to identify the IDIs of the first lobe, we will estimate statistics from a sample of only 2 IDIs. The two effects can be present at the same time, leading to IDI samples with (a) a very low number of IDIs spread extensively over the different lobes as a result of the low detection probability, and (b) a large degree of overlapping of the two first lobes as a result of the high CV.

B. Improvements of the MLE Algorithm

The MLE algorithm simultaneously addresses the above two issues: as the IDI distribution model with missing firings is being used for the derivation of the estimator, the overlapping effects are already considered within the formulation, while all the IDIs within the sample are employed for the final estimation (Fig. 11). This theoretical advantage is supported by the results. The MLE algorithm is less biased for lower firing detection probability values and for higher CV values than the MnT and EFE algorithms, hence is more accurate, both in the estimation of the mean IDI (Fig. 3) and in the estimation of the IDI SD (Fig. 4). In addition, relative to MnT and EFE the MLE has lower variability in estimation error of both IDI mean and IDI SD, hence, MLE is more precise. This is the case for all combinations of p and CV values tested here, and it is further supported by reliability results (Fig. 9) showing that MLE is reliable over a wider p-CV region than EFE and MnT algorithms. In fact, the MLE algorithm becomes significantly biased only for very low detection probability values $(p=0.2)$, where only around 10 IDIs are measured, and even in these conditions the bias exhibited is much lower than that of the MnT and EFE algorithms. Another noticeable result is that, in total detection conditions $(p=1.0)$, the MLE provides practically unbiased estimations with a lower error variability than the MnT and EFE algorithms.

The MLE algorithm also presents robust behavior when faced with an IDI sample whose PDF departs from normality. Even with an IDI PDF with skewness, the results show the MLE algorithm behaves well; its estimates are less biased than those of the MnT and EFE algorithms and the error variability is smaller (Figs. 5 and 6). This is important because in real MU firing patterns IDIs are distributed with low to moderate skewness [3], [25]. Although high asymmetry can result from nonstationarity conditions due to the experimental setup [1], [4], a certain degree of skewness can still be found in adequately recorded MU firing patterns and the MLE algorithm can handle this. In general, when skewness is present, the three algorithms underestimate the mean IDI for high p values, and overestimate it for low p values. While overestimation is explained, as in the case of normality, by scarceness and spread of IDI data, underestimation can be attributed to the positive skewness of the IDI distribution when a symmetric distribution is expected. It should be noted that the MLE framework could be easily extended to consider IDI distributions other than normal, and, for example, use of a gamma distribution for IDIs may adequately deal with skewness in certain data.

Assuming, now, a normal distribution for the MU firing pattern IDIs, there are some circumstances in which all the algorithms may fail. With detection probability values below about 0.2, even the MLE error distribution becomes positively biased and skewed, tending towards overestimation of the IDI mean and SD. This is a straightforward consequence of the scarceness of data (e.g., if $p = 0.2$ and $\mu = 70$ ms, the number of IDIs measured in a 5 s recording is around 14) combined with the spread of the surviving IDIs through the different lobes (e.g., if $p = 0.2$, the percentage of IDIs falling in the first five lobes is 20%, 16%, 13%, 10%, and 8%, respectively). The result is that the algorithms find it difficult to identify the main lobe. Note that, when $p = 0.2$, even an increase of the CV does not further worsen the estimation error distributions for the IDI mean of the three algorithms being compared (Fig. 3).

C. Applicability of the MLE Algorithm

When applied to real signals, the MLE algorithm demonstrates robust behavior with lower bias and error dispersion than the EFE and MnT algorithms, especially for MU firing patterns with low detection probability (Fig. 10). It should be noted that in real signals, stationarity is not ensured, and the IDI PDF may show a certain degree of skewness. Although highly nonstationary signals were excluded from our tests, signals showing slow trends on the mean firing rate were admitted. This highlights the robustness of the algorithm in real conditions. For levels of detection probability commonly experienced during EMG signal decomposition (p from 0.3 to 0.8) the MLE algorithm is more reliable than EFE and MnT (Fig. 9), especially for CV values over 0.2, which can be commonly encountered for MUs close to their recruitment threshold [2]. Hence, the MLE algorithm extends the range of signals for which a reliable estimation of mean and SD statistics can be obtained.

The main benefit of the MLE algorithm is demonstrated when testing the goodness-of-fit of the complete MU firing pattern to the distributions obtained with the estimated parameters from the incomplete MU firing pattern, $\hat{\mu}$ and $\hat{\sigma}$. The MLE algorithm estimates are rejected roughly once for each of the two rejections under the EFE and MnT algorithms. The cases where MLE fit is not rejected but EFE fit is rejected generally occur in a region with moderate detection probability (0.4 to 0.6) and moderate to low CV (0.1 to 0.2), which coincides with part of the region for which, in terms of IDI SD estimation, it is shown that MLE is reliable but EFE is not (Fig. 9). These results suggest that the main reason for the improved performance of the MLE algorithm over the EFE algorithm is a more reliable estimation of the IDI SD, especially in the above-defined region.

The nature of the challenge addressed here does not allow us to take advantage of some of the excellent properties of maximum likelihood estimators, such as, consistency, asymptotic normality and efficiency, which become useful for large samples in asymptotic conditions. In essence, it is the short duration of recordings (from 5 to 10 s) needed to ensure the stationarity of the firing generation process [1] that does not allow us to exploit the aforementioned benefits of maximum likelihood estimators with real signals. Simulations confirm that MLE results tends towards unbiasedness for large IDI samples, while EFE and MnT remain biased (Fig. 7).

Another important aspect when evaluating the applicability of an algorithm is its computational cost. In terms of computation time, MLE is slower than EFE and MnT algorithms. Despite this, the absolute computation times for the MLE, of about 6 ms per estimation for a 5 s length recording, are acceptable in most applications. In addition, note that the current MLE implementation was coded in Matlab and not optimized with computational efficiency in mind.

In terms of the MLE framework applicability, one possibility is to extend the model to incorporate skewness in the IDI distribution by means of a gamma PDF, as mentioned before. Another possibility is the specific incorporation of classification errors in the model. The EFE and MnT algorithms tend to exclude outliers by means of IDI thresholding, and this is an advantage over the MLE algorithm when dealing with shorter IDIs from doublets or classification errors. Incorporation of a full treatment of false positives into the IDI PDF model may optimize the MLE approach for situations with shorter IDIs. Both extensions of the framework (including skewness and classification errors) imply the incorporation of new parameters to the PDF model. These parameters would have to be estimated during the MLE process. Finally, the model-based approach used here could be extended to obtain full posterior distributions which may provide insight into parameter uncertainty.

V. Conclusion

A new method for the estimation of the IDI statistics based on MLE has been presented. The estimator is accurate and precise even with a high CV and low detection probability, outperforming previously developed algorithms. The estimator remained robust even with real IDI distributions with a certain amount of skewness. The accuracy and precision of the MLE algorithm is attributable to its use of all the IDI samples to fit a PDF model that incorporates the firing detection probability.

REFERENCES

[1] C. J. De Luca, "Physiology and mathematics of myoelectric signals," *IEEE Trans. Biomed. Eng.*, vol. 26, no. 6, pp. 313–325, Jun. 1979.

[2] H. P. Clamann, "Statistical analysis of motor unit firing patterns in a human skeletal muscle," *Biophys. J.*, vol. 9, no. 10, pp. 1233–1251, Oct. 1969.

[3] R. S. Person and L. P. Kudina, "Discharge frequency and discharge pattern of human motor units during voluntary contraction of muscle," *Electroencephalogr. Clin. Neurophysiol.*, vol. 32, no. 5, pp. 471–483, May 1972.

[4] K. B. Englehart and P. A. Parker, "Single motor unit myoelectric signal analysis with nonstationary data," *IEEE Trans. Biomed. Eng.*, vol. 41, no. 2, pp. 168–180, Feb. 1994.

[5] C. T. Moritz, B. K. Barry, M. A. Pascoe, and R. M. Enoka, "Discharge rate variability influences the variation in force fluctuations across the working range of a hand muscle," *J. Neurophysiol.*, vol. 93, no. 5, pp. 2449–2459, May 2005.

[6] M. A. Pascoe, M. R. Holmes, and R. M. Enoka, "Discharge characteristics of biceps brachii motor units at recruitment when older adults sustained an iometric contraction," *J. Neurophysiol.*, vol. 105, no. 2, pp. 571–581, Feb. 2011.

[7] D. W. Stashuk, "Decomposition and quantitative analysis of clinical electromyographic signals," *Med. Eng. Phys.*, vol. 21, no. 6, pp. 389–404, 1999.

[8] D. Stashuk, "EMG signal decomposition: How can it be accomplished and used?," *J. Electromyogr. Kinesiol.*, vol. 11, no. 3, pp. 151–173, June 2001.

[9] K. C. McGill, K. L. Cummins, and L. J. Dorfman, "Automatic decomposition of the clinical electromyogram," *IEEE Trans. Biomed. Eng.*, vol. 32, no. 7, pp. 470–477, Jul. 1985.

[10] J. R. Florestal, P. A. Mathieu, and A. Malanda, "Automated decomposition of intramuscular electromyographic signals," *IEEE Trans. Biomed. Eng.*, vol. 53, no. 5, pp. 832–839, May 2006.

[11] J. Florestal, P. Mathieu, and K. Mcgill, "Automatic decomposition of multichannel intramuscular EMG signals," *J. Electromyogr. Kinesiol.*, vol. 19, no. 1, pp. 1–9, 2009.

[12] H. Parsaei, D. W. Stashuk, S. Rasheed, C. Farkas, and A. Hamilton-Wright, "Intramuscular EMG signal decomposition," *Crit. Rev. Biomed. Eng.*, vol. 38, no. 5, pp. 435–465, 2010.

[13] D. Stashuk and Y. Qu, "Adaptive motor unit action potential clustering using shape and temporal information," *Med. Biol. Eng. Comput.*, vol. 34, no. 1, pp. 41–49, 1996.

[14] H. Parsaei, F. Nezhad, D. Stashuk, and A. Hamilton-Wright, "Validating motor unit firing patterns extracted by EMG signal decomposition," *Med. Biol. Eng. Comput.*, vol. 49, no. 6, pp. 649–658, 2010.

[15] K. C. McGill and H. R. Marated, "Rigorous *a posteriori* assesment of accuracy in EMG decomposition," *IEEE Trans. Biomed. Eng.*, vol. 19, no. 1, pp. 54–63, Feb. 2011.

[16] H. Parsaei and D. W. Stashuk, "A method for detecting and editing MUPTS contaminated by false classification errors during EMG signal decomposition," in *Proc. 33th IEEE Eng. Med. Biol. Soc. Conf.*, 2011, pp. 4394–4397.

[17] H. R. Marateb, S. Muceli, K. C. McGill, R. Merletti, and D. Farina, "Robust decomposition of single-channel intramuscular EMG signals at low force levels," *J. Neural. Eng.*, vol. 8, no. 6, p. 066015, Dec. 2011.

[18] H. Parsaei and D. W. Stashuk, "SVM-based validation of motor unit potential trains extracted by EMG signal decomposition," *IEEE Trans. Biomed. Eng.*, vol. 51, no. 1, pp. 183–191, Jan. 2012.

[19] H. Parsaei and D. W. Stashuk, "EMG signal decomposition using motor unit potential train validity," *IEEE Trans. Neural Syst. Rehabil. Eng.*, vol. 21, no. 2, pp. 265–274, Mar. 2013.

[20] K. C. McGill, "A method for quantitating the clinical electromyogram," Ph.D. dissertation, Stanford Univ., Stanford, CA.

[21] D. W. Stashuk and Y. Qu, "Robust method for estimating motor unit firing-pattern statistics," *Med. Biol. Eng. Comput.*, vol. 34, no. 1, pp. 50–57, 1996.

[22] H. S. Milner-Brown, R. B. Stein, and R. Yemm, "Changes in firing rate of human motor units during linearly changing voluntary contractions," *J. Physiol.*, vol. 230, no. 2, pp. 371–390, Apr. 1973.

[23] C. J. De Luca, P. J. Foley, and Z. Erim, "Motor unit control properties in constant-force isometric contractions," *J. Neurophysiol.*, vol. 76, no. 3, pp. 1503–1516, Sep. 1996.

[24] W. S. Masland, D. Sheldon, and C. D. Hershey, "Stochastic properties of individual motor unit interspike intervals," *Am. J. Physiol.*, vol. 217, no. 5, pp. 1384–1388, Nov. 1969.

[25] C. J. De Luca and W. J. Forrest, "Some properties of motor unit action potential trains recorded during constant force isometric contractions in man," *Kybernetik*, vol. 12, no. 3, pp. 160–168, Mar. 1973.

[26] S. Andreassen and A. Rosenfalck, "Regulation of the firing pattern of single motor units," *J. Neurol. Neurosurg. Psychiat.*, vol. 43, no. 10, pp. 897–906, Oct. 1980.

[27] F. Buchthal, P. Pinelli, and P. Rosenfalck, "Action potential parameters in normal human muscle and their physiological determinants," *Acta. Physiol. Scand.*, vol. 32, pp. 219–229, 1954.

[28] K. C. McGill, Z. C. Lateva, and H. R. Marateb, "EMGLAB: An interactive EMG decomposition program," *J. Neurosci. Methods*, vol. 149, no. 2, pp. 121–133, 2005.

[29] J. D'Errico, "Fminsearchbnd documentation," Aug. 11, 2005, 10 Oct. 2013 [Online]. Available: http://www.mathworks.com/matlabcentral/fileexchange/8277-fminsearchbnd-fminsearchcon

Javier Navallas was born in Pamplona, Spain, in 1976. He graduated in 2002, and received the Ph.D. degree in telecommunication engineering from the Public University of Navarra, Pamplona, Spain, in 2008.

He has worked as a Software Engineer. He is presently Associate Professor of the Electrical and Electronics Engineering Department, Public University of Navarra, Pamplona, Spain. His research interests are modeling of the neuromuscular systems and neural information processing.

Armando Malanda was born in Madrid, Spain, in 1967. He graduated in telecommunication engineering from the Madrid Polytechnic University, Madrid, Spain, in 1992, and received the Ph.D. degree from the Carlos III University, Madrid, Spain, in 1999.

In 1992 he joined the School of Telecommunication and Industrial Engineering, Public University of Navarra, Pamplona, Spain. In 2003 he became Associate Professor in the Electrical and Electronics Engineering Department of this University. During this period he has been teaching several subjects related to digital signal processing, image processing, and biomedical engineering. His areas of interest comprise the analysis, modeling and simulation of bioelectrical signals, particularly EEG and EMG.

Javier Rodriguez-Falces received the Ph.D. degree in electromyography from the Public University of Navarra, Pamplona, Spain, in 2007.

He is a Professor at the Department of Electrical and Electronic Engineering at the Public University of Navarra, Pamplona, Spain. He teaches courses in the Master of Biomedical Engineering and in the Bachelor Degree of Telecommunication. His research interests include biomedical signal processing, quantitative analysis of electromyographic signals, modeling, and analysis of muscle electrical and mechanical responses and neuromuscular adaptations to exercise.